



## The Taylor-vortex dynamo

Christophe Gissinger

Citation: *Physics of Fluids* (1994-present) **26**, 044101 (2014); doi: 10.1063/1.4869725

View online: <http://dx.doi.org/10.1063/1.4869725>

View Table of Contents: <http://scitation.aip.org/content/aip/journal/pof2/26/4?ver=pdfcov>

Published by the [AIP Publishing](#)

---

### Articles you may be interested in

[Electromagnetically driven dwarf tornados in turbulent convection](#)

*Phys. Fluids* **23**, 015103 (2011); 10.1063/1.3541817

[Stability of flow between two corotating disks in an enclosure](#)

*Phys. Fluids* **19**, 068106 (2007); 10.1063/1.2747543

[Finite-amplitude modulated Taylor-Couette flow](#)

*Phys. Fluids* **18**, 044105 (2006); 10.1063/1.2193473

[Taylor-Couette flow with an imposed magnetic field — linear and nonlinear results](#)

*AIP Conf. Proc.* **733**, 142 (2004); 10.1063/1.1832144

[Dynamo action in the Taylor–Green vortex near threshold](#)

*Phys. Plasmas* **4**, 1 (1997); 10.1063/1.872578

---



## Re-register for Table of Content Alerts

Create a profile.



Sign up today!



## The Taylor-vortex dynamo

Christophe Gissinger

*Laboratoire de Physique Statistique, Ecole Normale Supérieure, CNRS, 24 rue Lhomond, 75005 Paris, France*

(Received 24 December 2013; accepted 12 March 2014; published online 1 April 2014)

The generation of a magnetic field by dynamo action in a Taylor-vortex flow is investigated numerically. We first discuss how the Taylor vortices generate a spatially subharmonic dynamo, for which the axial wavelength of the magnetic field is twice the one of the flow pattern. Then, we investigate the influence of the Reynolds number and the turbulent fluctuations on the structure and the onset of the Taylor-Couette dynamo. Finally, based on the subharmonic nature of this dynamo, we propose new configurations which could be relevant for laboratory experiments. © 2014 AIP Publishing LLC. [<http://dx.doi.org/10.1063/1.4869725>]

### I. INTRODUCTION

It is now commonly believed that most of the astrophysical magnetic fields are due to dynamo action, i.e., the self-generation of a magnetic field by the motion of a turbulent electrically conducting fluid.<sup>1</sup> Most of the planetary and stellar dynamos can be described by cellular motions of a fluid confined inside a spherical shell in strong rotation, modeling the convection zone of astrophysical objects. In the case of galaxies and accretion discs, a cylindrical geometry is more appropriate, and these astrophysical systems can be idealized by a magnetized Taylor-Couette flow, i.e., the viscous flow of an electrically conducting fluid confined between two differentially rotating concentric cylinders.<sup>2</sup>

During the last decades, the dynamo problem has greatly benefited from numerical simulations, especially concerning dynamos generated by laminar flows. However, a lot of questions remain concerning the generation of a dynamo magnetic field when the flow is strongly turbulent. On the other hand, the Taylor-Couette (TC) flow is among the most studied problems in unmagnetized fluid dynamics and has been largely studied in the framework of turbulence. Surprisingly, only a few numerical work has been done on dynamos generated by Taylor-Couette flows.

The Taylor-Couette dynamo has been studied only recently. Willis and Barhengi,<sup>3</sup> in 2002, investigated numerically the generation of a nonlinear dynamo in an axially periodic Taylor-Couette flow, extending a theoretical study of Laure *et al.*<sup>4</sup> It was shown that a non-axisymmetric magnetic field can be generated by the axisymmetric Taylor vortices arising from the centrifugal instability of the circular Couette flow. Laguerre *et al.*<sup>5</sup> reproduced these results using more realistic boundary conditions at the endcaps of the cylinders (finite cylinders). Although the latter study was done in a laminar regime, it was shown that a complex time behavior of the  $m = 1$  dynamo can be obtained. In a recent laboratory experiment, Colgate *et al.*<sup>6</sup> showed that the differential rotation in Taylor-Couette flows yields a very strong induction of the magnetic field by  $\omega$ -effect. Apart from its ability to generate dynamo action, the magnetized Taylor-Couette flow also constitute a generic model for the magneto-rotational instability (MRI), and is currently studied by several experiments.<sup>7</sup>

In the present work, we extend these previous studies by investigating numerically the generation of a dynamo magnetic field in a turbulent Taylor-Couette flow with finite-size cylinders. In the first part of the article, we report calculations in the laminar regime and discuss the subharmonic nature of the Taylor-Couette dynamo. In the second part of the paper, the Reynolds number  $Re$  is varied on a relatively large range, and we show how the structure and the onset of the dynamo magnetic field are modified by turbulent fluctuations. Finally, by varying the aspect-ratio between the cylinders

and the boundary conditions at the endcaps, we discuss the relevance of the Taylor-Couette flow for laboratory experiments, and propose new types of configurations.

## II. MODEL

We consider the flow of an electrically conducting fluid between two co-rotating finite cylinders.  $r_1$  is the radius of the inner cylinder,  $r_2 = r_1/\eta$  is the radius of the outer cylinder, and  $d = r_2 - r_1$  is the gap between cylinders.  $\Omega_1$  and  $\Omega_2$  are respectively the angular speed of the inner and the outer cylinder. Depending on the configuration, the endcaps at the top and bottom boundaries can rotate either with the inner cylinder or with the outer one. The height of the cylinders  $H$  is changed such that the aspect ratio  $\Gamma = H/d$  varies between 3 and 8. In all the results reported here,  $\Omega_2$  is fixed to zero: only the inner cylinder is rotating.

The governing equations are the magnetohydrodynamic (MHD) equations, i.e., the Navier-Stokes equation coupled to the induction equation:

$$\rho \frac{\partial \mathbf{u}}{\partial t} + \rho (\mathbf{u} \cdot \nabla) \mathbf{u} = -\nabla P + \rho \nu \nabla^2 \mathbf{u} + \mathbf{j} \times \mathbf{B}, \quad (1)$$

$$\frac{\partial \mathbf{B}}{\partial t} = \nabla \times (\mathbf{u} \times \mathbf{B}) + \frac{1}{\mu_0 \sigma} \nabla^2 \mathbf{B}, \quad (2)$$

where  $\rho$  is the density,  $\nu$  the kinematic viscosity,  $\sigma$ , the electrical conductivity,  $\mu_0$  the magnetic permeability,  $\mathbf{u}$  is the fluid velocity,  $\mathbf{B}$  the magnetic field, and  $\mathbf{j} = \mu_0^{-1} \nabla \times \mathbf{B}$  the electrical current density. In addition to the geometrical parameters  $\Gamma$  and  $\eta$ , our problem can be characterized by two more dimensionless numbers: the fluid Reynolds number  $Re = (\Omega_1 r_1 d)/\nu$  and the magnetic Reynolds number  $Rm = (\Omega_1 r_1 d)\sigma \mu_0$ . It is also useful to define the magnetic Prandtl number  $Pm = \nu \sigma \mu_0$ , which is simply the ratio between the two Reynolds numbers.

These equations are integrated with the HERACLES code.<sup>8</sup> Originally developed for radiative astrophysical and ideal-MHD flows, it was modified to include viscous and magnetic diffusions. Note that HERACLES is a compressible code, whereas laboratory experiments generally involve almost incompressible liquid metals. In fact, incompressibility corresponds to an idealization in the limit of infinitely small Mach number ( $Ma$ ). In the simulations reported here, we used an isothermal equation of state with a small sound speed such that  $Ma < 0.3$ , following an approach known to efficiently simulate incompressible MHD Taylor-Couette flows.<sup>9–11</sup> Typical resolutions used in the simulations reported in this article range from  $(N_r, N_\phi, N_z) = [64, 128, 128]$  for laminar flows to  $(N_r, N_\phi, N_z) = [128, 256, 512]$  for the highest Reynolds numbers. The magnetic field is forced to be normal to the boundaries, describing ferromagnetic boundary conditions (sometimes referred as pseudo-vacuum conditions in the literature). For the velocity field, no-slip conditions are used for radial and axial components, whereas the angular velocity matches the rotation rates of corresponding boundaries.

For infinitely long cylinders, the ideal laminar Couette solution is given by

$$\Omega(r) = A_1 + \frac{A_2}{r^2} \quad (3)$$

in which  $A_1 = (\Omega_2 r_2^2 - \Omega_1 r_1^2)/(r_2^2 - r_1^2)$  and  $A_2 = r_1^2 r_2^2 (\Omega_1 - \Omega_2)/(r_2^2 - r_1^2)$ . The Rayleigh criterion predicts axisymmetric linear stability if  $\Omega_2/\Omega_1 \geq (r_1/r_2)^2$ , ensuring that the specific angular momentum increases outward. Otherwise, the centrifugal instability is observed, and takes the form of axisymmetric vortices contained in the poloidal  $(r, z)$  plane. When considering a realistic situation, two main effects are observed. First, the viscosity stabilizes the centrifugal instability, and the destabilization of the flow depends on the fluid Reynolds number  $Re$ . Second, no-slip boundary conditions at the vertical boundaries (for instance endcaps rigidly attached to either outer or inner cylinder) induce an imbalance between the pressure gradient and the centrifugal force, and drive a meridional Ekman recirculation in addition to the azimuthal Couette flow. In the case of stationary endcaps, an inward boundary-layer flow near the endcaps is balanced by strong outward jet at the midplane, even for Rayleigh-stable flows. This recirculation makes the hydrodynamic bifurcation of the Taylor-vortex flow strongly imperfect.<sup>12</sup>

### III. LAMINAR DYNAMO

It is known that the ideal circular Couette solution (3) cannot generate a magnetic field by dynamo action. There are therefore two ways to destabilize this flow. First, in the Rayleigh-stable regime, it is possible to destabilize the flow through the magneto-rotational instability (MRI).<sup>13</sup> Some studies suggest that the MRI-driven turbulence is then able to sustain a dynamo magnetic field.<sup>14</sup> However, this scenario can be observed only at relatively large  $Rm$  which are out of range of laboratory experiments and which will not be considered here. On the other hand, if the flow is Rayleigh-unstable, for instance if only the inner cylinder is rotating, a dynamo magnetic field can be sustained by the Taylor vortices created by the centrifugal instability. In this case, there is always a critical Reynolds number  $Re_c$  corresponding to the bifurcation of Taylor vortices below which no dynamo can be obtained, independently of the value of  $Rm$ . In the present work, we have chosen to put the rotation rate of the outer cylinder to zero and the radius ratio  $\eta = r_1/r_2$  to 0.5. For the parameters used in this paper, and for infinite cylinders, the axisymmetric Taylor vortices appear from a perfect supercritical bifurcation at  $Re_c \sim 68$ , with an axial wavenumber  $k_V = 3.14$ , corresponding to almost *square* cells.<sup>15</sup> Note that all the previous numerical studies of the Taylor-Couette dynamo have been restricted to values relatively close to  $Re_c$ , for which the Taylor-Couette flow is laminar.

As the distance from the hydrodynamic threshold  $Re - Re_c$  is increased, the amplitude of the vortices becomes large enough to sustain a dynamo magnetic field, as shown in Fig. 1. This figure shows the typical structure of velocity and magnetic fields obtained for  $Re = 130$  and  $Rm = 200$ . On the left is shown the structure of the velocity field in the  $(r, z)$ -plane, in the case of axially periodic cylinders. The colorplot shows the radial velocity field, and the lines indicate streamline in this poloidal plane.

For  $\Gamma = 4$ , the Taylor vortices take the form of two pairs of rolls (4 vortices) contained in the poloidal plane, associated with strong outflows, periodically arranged. The middle figure shows the azimuthal magnetic field in the same  $(r-z)$  plane. The magnetic eigenmode consists of a non-axisymmetric regular  $m = 1$  pattern, as shown by the isosurface of the magnetic energy in Figure 1(right).

In the context of experimental dynamos, it is crucial to understand how the Taylor-Couette dynamo is modified when the axially periodic cylinders are replaced by finite-size cylinders with top and bottom endcaps. With finite cylinders, the aspect ratio  $\Gamma = H/d$  plays a determinant role in the generation of the dynamo magnetic field. Figure 2(left) shows how the critical magnetic Reynolds number needed for dynamo action evolves with the aspect ratio of the finite cylinders. At large values of  $\Gamma$ , the critical  $Rm$  is relatively low:  $Rm_c \sim 138$  for  $\Gamma = 8$ . As  $\Gamma$  is decreased, the critical  $Rm$  increases and finally diverges close to  $\Gamma = 3.5$ . For  $\Gamma = 3$ , no dynamo action has been observed for the magnetic Reynolds numbers investigated ( $Rm < 1000$ ). These results indicate that large aspect-ratio Taylor-Couette flow may be more prone to dynamo action than short aspect ratio devices. Apart from this general behavior, the stability curve also exhibits small modulations, with several local decreases of  $Rm_c$  at particular values of  $\Gamma$ , for instance around  $\Gamma = 4$  or  $\Gamma = 7$ .

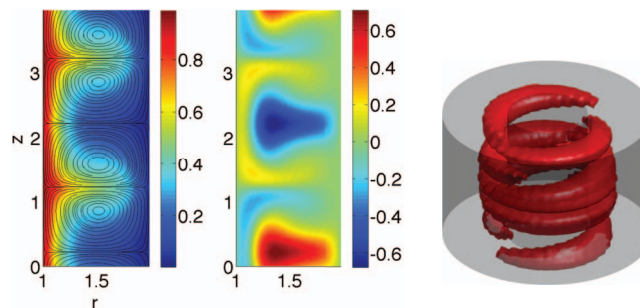


FIG. 1. Structure of the Taylor-Couette dynamo in the laminar regime, for  $Re = 130$  and  $Rm = 200$ . Left: Colorplot of the velocity field in the poloidal  $(r, z)$  plane, showing the Taylor vortices. Middle: Colorplot of the azimuthal magnetic field. Right: Isosurface of the magnetic energy of the  $m = 1$  dynamo mode.

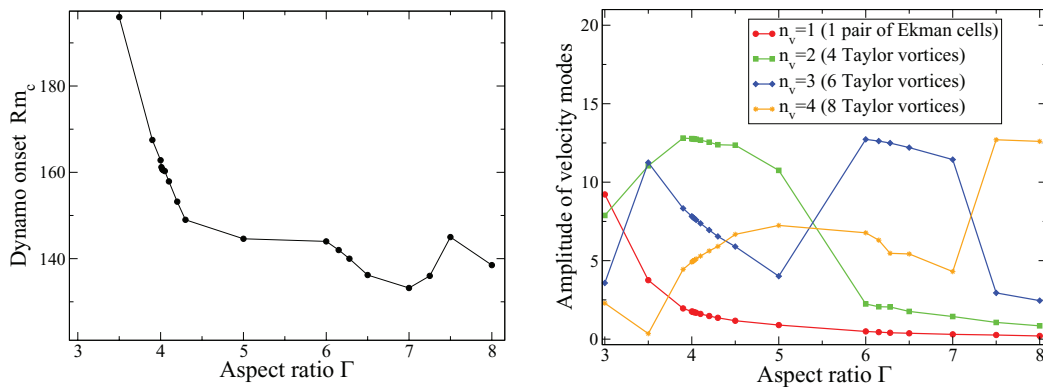


FIG. 2. Left: Critical  $Rm$  for dynamo action versus  $\Gamma$ . Note the divergence of the dynamo threshold at  $\Gamma \sim 3$ . Right: Amplitude of the Fourier components in the axial direction of the velocity field, as a function of the aspect ratio  $\Gamma$ .

This behavior is in fact strongly related to the axial structure of the velocity field, as shown in Fig. 2(right). In this figure, we plotted the saturated amplitude of the different velocity Fourier modes in the  $z$ -direction, as a function of  $\Gamma$ . For  $\Gamma = 8$ , exactly 4 pairs of *square* Taylor vortices can be arranged in the gap, leading to a strong amplitude of the axial Fourier velocity mode  $n_v = L/\lambda = 4$  (yellow-star symbols). As  $\Gamma$  is decreased, other resonances are obtained for  $\Gamma = 6$  (3 pairs of vortices) and  $\Gamma = 4$  (2 pairs of vortices), associated respectively with strong amplitudes of  $n_v = 3$  (blue-diamond curve) and  $n_v = 2$  (green-square curve) axial Fourier modes. On the other hand, the no-slip boundaries of the vertical endcaps always generate a strong Ekman pumping, taking the form of a  $n_v = 1$  mode (red-circle symbols), which modifies the Taylor vortices and becomes more and more important at shorter aspect ratio. Finally, when  $\Gamma < 3$ , the vertical extension of the gap is too small to sustain a Taylor vortex pattern, and only the strong  $n_v = 1$  Ekman flow remains.

To understand why this 2-cells Ekman flow is unable to generate a dynamo at low  $Rm$ , we now turn to Fig. 3. In this figure, we have plotted the axial profiles of the three components of the velocity field together with the azimuthal magnetic field, for periodic (top) and finite cylinders with  $\Gamma = 4$  (middle) and  $\Gamma = 8$  (bottom). First, comparison of top and middle figures shows that vertical endcaps only slightly modify the flow, the main differences occurring near the endcaps, where the velocity field is forced to be zero in the case of finite cylinders.

The middle and bottom figures then compare calculations with different aspect ratios. Since the wavelength of Taylor cells is twice the gap in both cases, a  $n_v = 4$  velocity mode is generated for  $\Gamma = 8$  whereas a  $n_v = 2$  mode is obtained for  $\Gamma = 4$ . Despite this difference, the generated magnetic field (blue-dark line) is growing in both cases at twice the wavelength of the velocity field

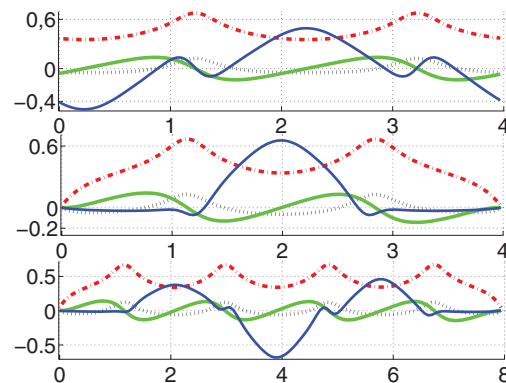


FIG. 3. Axial profiles of velocity components  $u_\phi$  (dash-dot red curve),  $u_r$  (dot-black),  $u_z$  (green-light) and dynamo radial magnetic field (blue-dark) in the case of axially periodic cylinders (top), and finite cylinders with  $\Gamma = 4$  (middle) or  $\Gamma = 8$  (bottom). The figure illustrates the subharmonic structure of the dynamo.

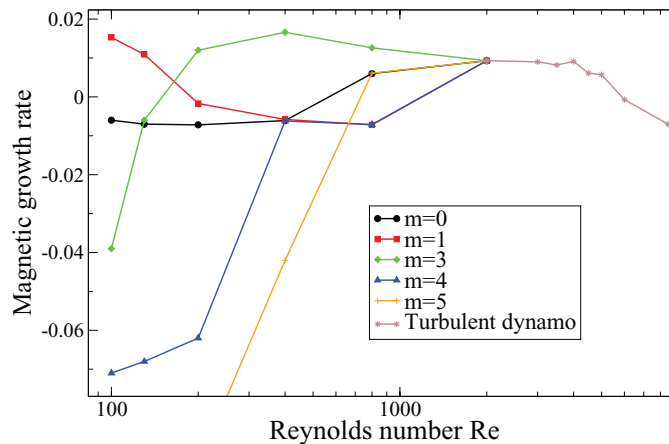


FIG. 4. Evolution of the growth rate of the azimuthal Fourier modes of the magnetic energy, as a function of  $Re$ , for a fixed value of  $Rm = 200$ .

( $n_b = 1$  or  $n_b = 2$ ). The Taylor-Couette flow, at least in this laminar regime, therefore generates a subharmonic dynamo. This is in contrast with most dynamos associated to cellular motions, for which the harmonic response is in general the most unstable mode. In the Roberts flow for instance, it was shown that subharmonic dynamos can be observed but, except for one special case, these modes always appear at higher magnetic Reynolds numbers than harmonic modes.<sup>16,17</sup>

This subharmonicity also explains the behavior of the marginal stability curve of Fig. 2: when the aspect-ratio is too small, the Taylor vortices are inhibited and the  $n_v = 1$  Ekman flow is enhanced, which prevents the generation of any subharmonic dynamo mode. When  $\Gamma$  is increased beyond 3, Taylor vortices are excited, thus allowing the generation of a subharmonic dynamo magnetic field.

It is well known that apart from this general behavior, marginal stability lines of hydrodynamical instabilities can exhibit resonant tongues due to finite-size effects, the Faraday instability being the most famous example. It is interesting to note that in our case, the dynamo field corresponds to a secondary bifurcation but its stability curve still exhibits this characteristic non-monotonic behavior, reminiscent from the resonance conditions of the primary bifurcation due to centrifugal instability.

Finally, note that for  $\Gamma < 3$ , one could expect a harmonic magnetic field to be generated by the  $n_v = 1$  Ekman flow, similarly to the Dudley and James dynamo generated by  $s_1^0 t_1^0$  flow. However, it has been recently shown<sup>18</sup> that such short aspect ratio Taylor-Couette systems generate flows with poloidal/toroidal ratios strongly unfavorable to dynamo action, unless a body force is artificially added to the equations. In the last section of this article, we will see how the subharmonic nature of the Taylor-Couette dynamo can be used to produce very efficient dynamo configurations.

#### IV. TURBULENT DYNAMO

Although Sec. III clearly demonstrates the ability of the Taylor-Couette flow to sustain a dynamo magnetic field, it is very difficult to extrapolate these results to a laboratory experiment. Indeed, due to the extremely weak value of the magnetic Prandtl number  $Pm$  in liquid metals, most of natural and experimental dynamos are generated from very turbulent flows, involving Reynolds numbers of several millions. It is therefore important to understand how the Taylor-Couette dynamo is modified as the level of turbulent fluctuations in the flow is increased. In particular, it is known that when  $Re$  exceeds a few thousands or so, the Taylor-Couette flow undergoes a transition to a turbulent state, in which the Taylor vortex structure is recovered only through time or azimuthal average.

To follow the effect of this transition on the dynamo, Fig. 4 shows the growth rate of the magnetic energy modes as a function of the Reynolds number, for  $Rm = 200$  and  $\Gamma = 2\pi$ . As  $Re$  is increased (at fixed  $Rm$ ) beyond its critical value for the bifurcation of Taylor vortices ( $Re \sim 68$ ), the amplitude of the flow increases until the Taylor vortices are able to sustain a dynamo magnetic field. This occurs for  $Re_c \sim 90$ . As described above, the dynamo magnetic field takes the form of a

$m = 1$  mode. If  $Re$  is increased further, the growth rate of the  $m = 1$  magnetic mode decreases and finally becomes negative for  $Re \sim 200$ . On the other hand, the growth rate of the  $m = 2$  magnetic mode increases and becomes positive approximately for the same  $Re$ . In the nonlinear regime, this transition takes the form of a secondary bifurcation, in which the  $m = 1$  mode is replaced by an  $m = 2$  magnetic field. In the kinematic results of Willis and Barhengi,<sup>3</sup> in which the azimuthal wavenumber  $m$  was restricted to a given value, it was shown that the dynamo tends to be restabilized at large  $Re$  if the outer cylinder is stationary. In the simulations reported here, we observe a similar tendency of the  $m = 1$  magnetic mode to be restabilized at large  $Re$ . But since the  $m = 2$  mode takes over at large  $Re$ , the dynamo is maintained.

For larger  $Re$ , the linear growth rate of the magnetic field slightly increases, but the structure remains identical. However, for  $Re \sim 2000$ , a sharp transition occurs in the velocity field, and the Taylor-Couette flow becomes more turbulent. This purely hydrodynamical transition of the laminar Taylor vortices to a chaotic flow has been largely described in the literature.

Figure 5 shows the velocity field obtained beyond the transition, for  $Re = 5000$ . Although not fully turbulent, the flow exhibits a very chaotic structure in both space and time, characterized by strong non-axisymmetric components and the presence of small scale vortices close to the inner cylinder (see colorplot of  $V_\phi$ ). These structures may be related to formation of Gortler vortices, known to appear from Taylor-Couette flow at sufficiently large  $Re$ .

Interestingly, a magnetic field is still self-generated in this new chaotic regime. During the kinematic stage, all the different azimuthal modes show a similar growth rate, illustrating the turbulent nature of the dynamo, which cannot be described as a given azimuthal Fourier mode since the eigenmode has projections in the whole Fourier space. In the rest of the paper, we will denote this dynamo as a *turbulent* Taylor-Couette dynamo.

Figure 6 shows the time evolution of this turbulent dynamo. At the beginning of the simulation, the flow is strongly chaotic and no organized patterns can be observed in the velocity field. After some transient time  $\tau$  (typically a viscous time), a transition occurs in the flow. For instance, for  $Re = 5000$ , Fig. 6 shows that after  $t \sim 1000$ , the axisymmetric component of the velocity field (top black curve) suddenly increases whereas non-axisymmetric modes decrease. This corresponds to the recovery of an organized vortex flow, although strongly fluctuating. The instantaneous flow is still chaotic, but the mean flow (averaged in time and along the azimuthal direction) exhibits poloidal structures similar to laminar Taylor vortices.

Figure 6(right) shows the evolution of the magnetic field during this transition. For  $t < 1000$ , when the flow is strongly chaotic, the magnetic energy rapidly decreases without any spatial structure. However, as soon as the hydrodynamic transition occurs, both the growth rate and the structure of the magnetic field suddenly change. We then observe an exponentially growing dynamo magnetic field, strongly fluctuating, and still dominated by an  $m = 2$  mode. Figure 7 shows the magnetic field obtained in this turbulent regime. The  $m = 2$  component of the magnetic field is quite clear, but the field in the poloidal plane is less organized, and exhibits a chaotic structure, fluctuating in time, with strongly localized patches of magnetic energy (here at  $z \sim 4.5$  for instance).

These results suggest that the velocity field responsible for the growth of the dynamo magnetic field in this chaotic regime is still the Taylor vortex structure of the mean flow. This is confirmed by Fig. 8, which reports the structure of the flow averaged both in time and in the azimuthal direction for  $Re = 5000$  (for which a dynamo was obtained at  $Rm = 200$ ) and for  $Re = 8500$  (for which no dynamo was found at  $Rm = 200$ ). These two cases are compared with the laminar solution obtained at  $Re = 130$ , independent of time and  $\phi$ . At  $Re = 5000$ , the averaged flow exhibits a structure very similar to the laminar solution, characterized by 3 pairs of Taylor vortices. At  $Re = 8500$ , the mean flow is significantly less organized and the coherence of the Taylor vortices is weaker due to turbulent fluctuations. Such a competition between a mean flow dynamo mode and a fluctuation dynamo mode has been discussed in previous studies.<sup>19-21</sup> Here, it seems that the turbulent fluctuations essentially decrease the dynamo efficiency of the mean Taylor-vortex flow.

Finally, when  $Re$  is increased further, the typical time  $\tau$  after which the Taylor vortex mean flow emerges becomes larger than the simulation time (see inset of Fig. 6). Therefore, for  $Re > 6000$ , the magnetic growth rate stays negative and no dynamo action is obtained for  $Rm = 200$ , as shown in Fig. 4. This is a dramatic illustration of the effect of the Reynolds number on the dynamo onset,

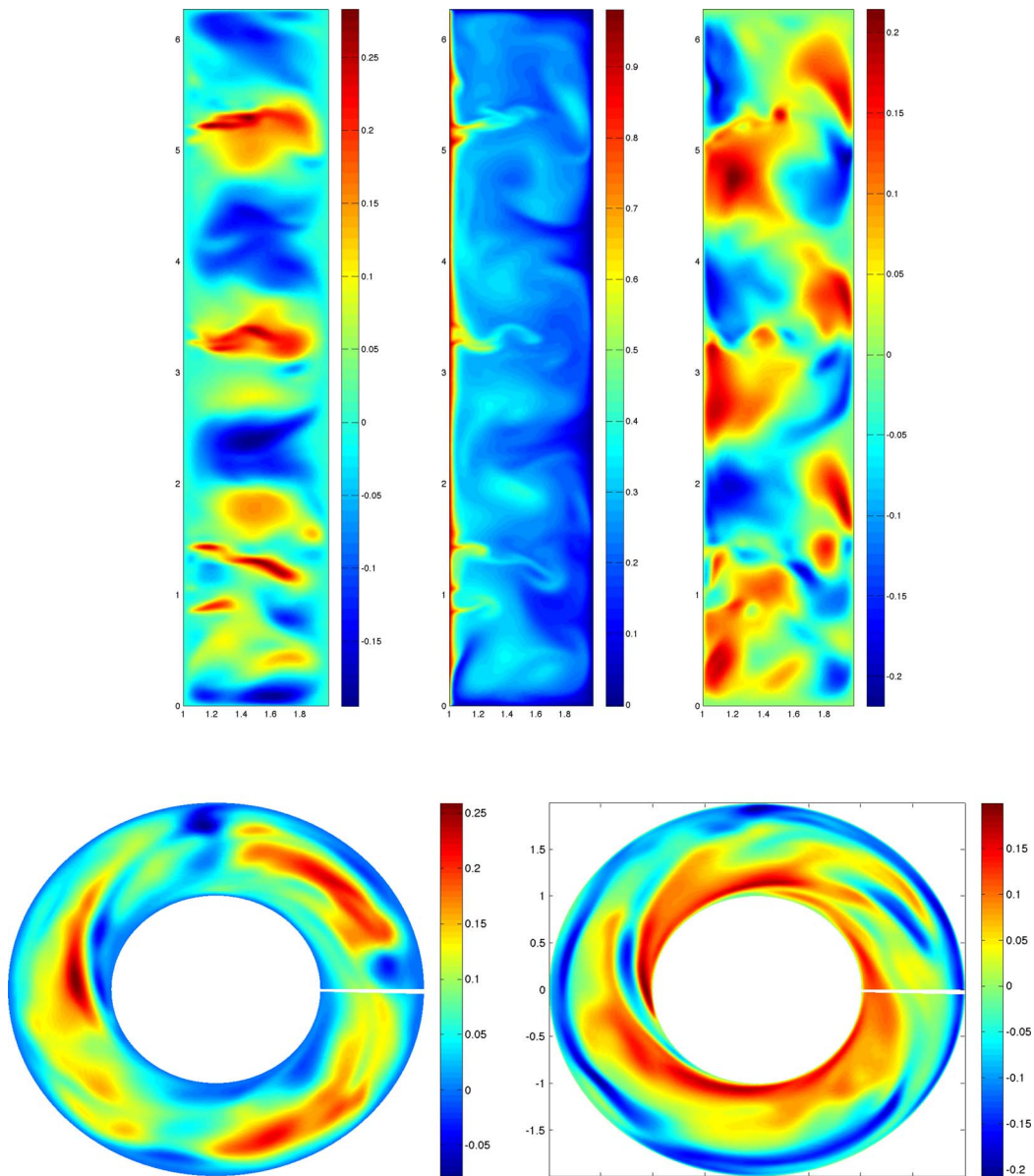


FIG. 5. Instantaneous velocity field in the purely hydrodynamical regime, when  $Re = 5000$ . Top: Colorplot showing the magnitude of the radial (left), azimuthal (middle), and axial(right) components of the flow in the  $(r, z)$  plane. Bottom: Same thing in the  $(r, \phi)$  plane for the radial(left) and axial(right) components.

the turbulent fluctuations increasing the critical magnetic Reynolds number  $Rm_c$ . It is not surprising since such a turbulent flow is characterized by the absence of coherent Taylor vortices, which have been shown to be crucial for the generation of the magnetic field. However, it is a strong obstacle to the success of laboratory dynamos expected to operate at very large  $Re$  but moderate  $Rm$ . This point is therefore discussed in Sec. V.

## V. ARTIFICIAL TAYLOR VORTICES

Sections II–IV demonstrate the ability of the Taylor-Couette flow to generate dynamo action at relatively low  $Rm$ , in both laminar and weakly turbulent regimes. At this point, it is thus interesting

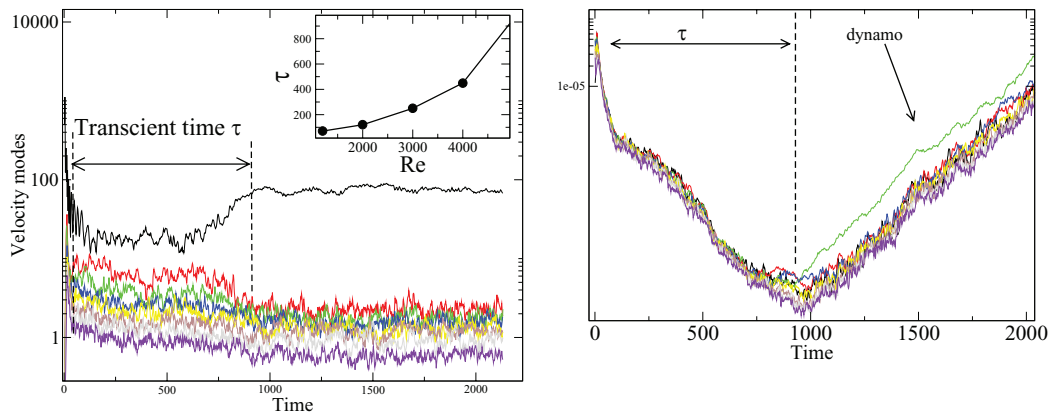


FIG. 6. Time evolution of the turbulent Taylor-Couette dynamo at  $Re = 5000$  and  $Rm = 200$  for different azimuthal wavenumber of the velocity field(left) and magnetic field (right).Inset: Evolution of the transient time  $\tau$  versus  $Re$ . Black, red, green, and blue colors respectively corresponds to  $m = 0, m = 1, m = 2$ , and  $m = 3$  azimuthal modes.

to discuss the possibility of observing such a dynamo in a laboratory experiment. During the last ten years, the experimental study of dynamo action has undergone significant developments.

In 1999, the first fluid dynamos have been obtained in Riga<sup>23</sup> and Karlsruhe<sup>22</sup> experiments, in which large scale turbulent fluctuations were reduced by some geometrical constraint. In 2006, the VKS experiment<sup>24</sup> showed that a fully turbulent flow can also generate a dynamo in a von Karman flow. However, the VKS dynamo is observed only when ferromagnetic discs are used, introducing a non-homogeneous distribution of magnetic permeability. It is therefore crucial to observe a laboratory dynamo magnetic field generated by an unconstrained and homogeneous flow.

The results reported in this article describes two types of dynamo which could be important for laboratory experiments. First, the dynamo observed in the laminar regime is more relevant to plasma experiments, in which the flow is expected to be laminar. The on-going Madison Plasma Couette experiment<sup>25</sup> is an example of such a laboratory experiment, which could lead to the generation of the  $m = 1$  or  $m = 2$  Taylor-Couette dynamos described in the first part of the paper. On the other hand, the fluctuating dynamo observed at large  $Re$  is more likely to be generated in a liquid metal experiment, where the flow is strongly turbulent. Our simulations however suggest that the coherence and the strength of the Taylor vortices are crucial to an efficient dynamo action, two effects possibly inhibited in a laboratory experiment. Indeed, Taylor vortices arise from an instability of the Couette flow, and their amplitude stays relatively small compared to the azimuthal Couette flow. In addition,

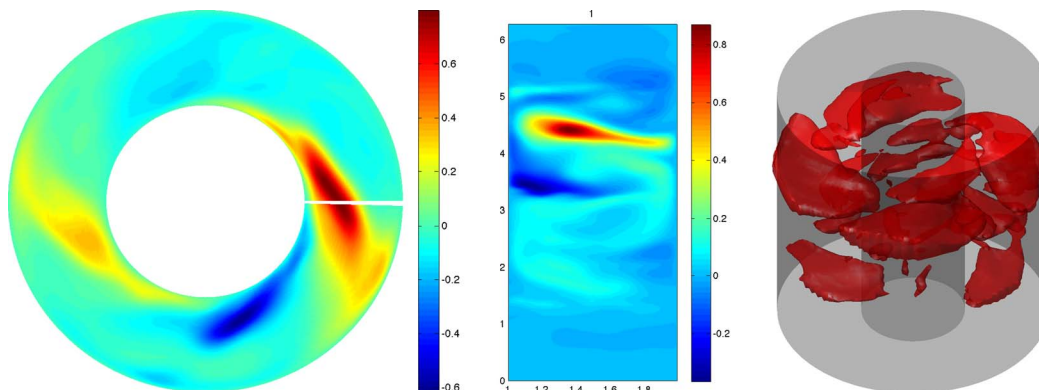


FIG. 7. Structure of the Taylor-Couette dynamo in the turbulent regime, for  $Re = 5000$  and  $Rm = 200$ . The figure shows a colorplot of the radial magnetic field in the  $(r, \phi)$  plane (left) and in the  $(r, z)$  plane (middle). Right: Isovalue of the magnetic energy.

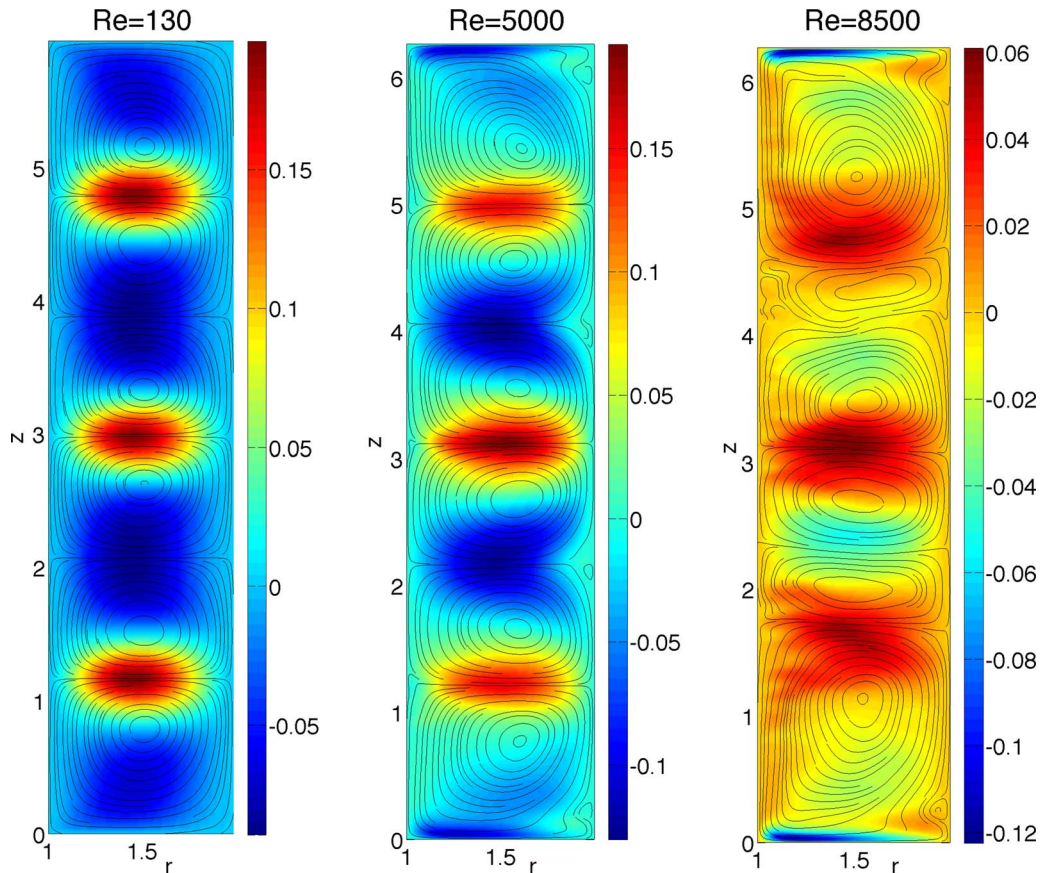


FIG. 8. Colorplot and streamlines of the poloidal velocity field averaged both in time and in the  $\phi$ -direction for  $Re = 130$  (left),  $Re = 6500$  (middle), and  $Re = 8500$  (right). At  $Rm = 200$ , no dynamo is observed for  $Re = 8500$ , whereas a dynamo is generated for  $Re = 5000$ , when the averaged flow is very close to the laminar  $n_v = 3$  Taylor vortex solution obtained at  $Re = 130$ .

when the flow becomes turbulent, the coherence of Taylor vortices is destroyed in the instantaneous flow, leading to a strong increase of the dynamo onset with  $Re$ . In the following, we therefore present how some simple modifications of the Taylor-Couette flow, based on the subharmonic nature of the dynamo, may help circumvent the problems mentioned above.

We have seen that the subharmonic dynamo needs at least 4 Taylor cells to be generated. It is possible to reinforce the production of these Taylor vortices by attaching additional annulus to the cylinders, as shown in the picture of Fig. 9(left). In the most simple case (case A), an annulus in the midplane is attached to the outer stationary cylinder, and extends radially almost to the inner cylinder. This procedure is equivalent to stack two small aspect-ratio Taylor-Couette devices with  $\Gamma = 2$  one on top of the other. The endcaps are at rest with the outer cylinder. In each compartment, the rotation of the inner cylinder generates a strong  $n_v = 1$  Ekman flow. This is therefore equivalent to 4 Taylor cells, producing an artificial  $n_v = 2$  flow able to sustain the subharmonic  $n_b = 1$  dynamo field. The second configuration (case “B”) is almost equivalent, except that both endcaps and the central ring are rotating with the inner cylinder, thus changing the direction of rotation (and the magnitude) of the artificial Taylor vortices (the flow is strongly ejected near endcaps). Finally, in the third configuration (case “C”), three rings are attached to cylinders such that each of the four compartments generates one vortex.

We have simulated each of these configurations by adding artificial boundaries at the location of the rings. In our numerical simulations, these rings have the same electrical conductivity and magnetic permeability than the fluid. The results are shown in Fig. 9(right), for  $Re = 130$  and  $\Gamma = 2\pi$ . Case “TC” (black-circle curve) indicates the classical Taylor-Couette dynamo discussed in

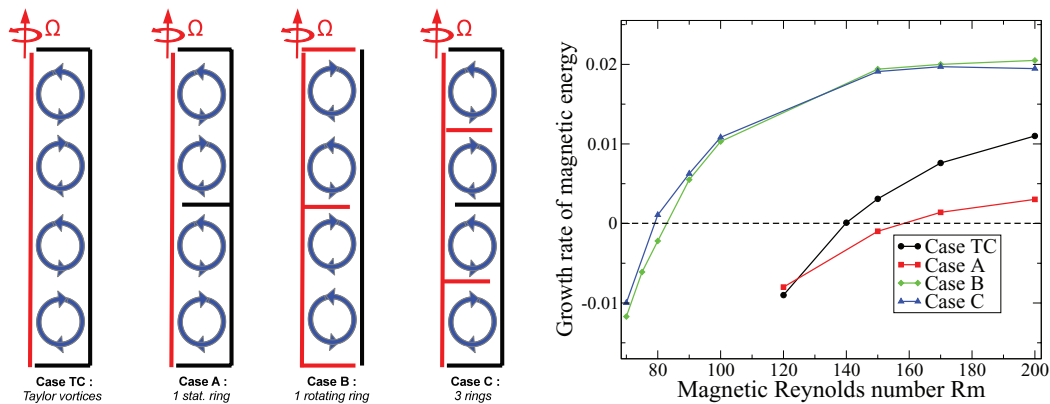


FIG. 9. Left: Schematic picture of the poloidal velocity obtained in the different configurations (see text). Right: Growth rate of the magnetic energy versus  $Rm$  for the different configurations.

Secs. II–IV. If case *A* (red-square) yields a critical dynamo onset higher than the Taylor-Couette flow, it is interesting to note that cases *B* (green-diamond), and *C* (blue-triangle) are much more favorable to dynamo action. The case *B* has a critical magnetic Reynolds number  $Rm_c \sim 85$ , which is 40% less than the classical Taylor-Couette flow. This can be explained by the difference in the amplitude of the generated vortices: with rotating endcaps, each compartment is associated with a strong Ekman recirculation, in which the flow close to the boundaries is strongly expelled outward by centrifugal force. The generated vortices are therefore much stronger than the Taylor vortices produced by Rayleigh instability, and this cellular flow characterized by  $n_v = 2$  is much efficient to produce the  $n_b = 1$  subharmonic dynamo. The case *C* is based on a similar effect, but with even stronger velocities and a dynamo onset around  $Rm_c = 80$ .

Figure 10 shows the structure of both velocity and magnetic fields for case *B*. As shown by Fig. 10(left), the rotation of the central ring and the endcaps produces 4 recirculation cells, very similar to the  $n_v = 2$  Taylor vortex flow. Similarly to the Taylor-couette dynamo (compare to Fig. 1), the magnetic field takes the form of a non-axisymmetric  $m = 1$  mode. Again, the dynamo is spatially subharmonic, growing with a vertical wavenumber  $k_b = k_v/2 = 1$  and with magnetic energy localized at the local minima of the azimuthal flow. Note that a classical Taylor-Couette device can easily be modified in order to produce the configurations proposed here.

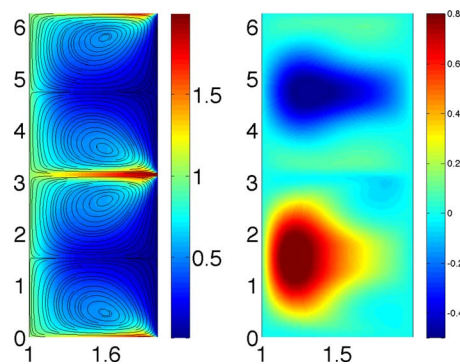


FIG. 10. Structure of the artificial Taylor vortex dynamo (case *B*). Left: Colorplot of the azimuthal velocity. The poloidal streamlines show the Taylor vortex-like patterns of the meridional recirculation. Right: Colorplot of the azimuthal magnetic field. Note the analogy with the Taylor-Couette dynamo shown in Fig. 1

## VI. CONCLUSION

In this article, we have reported direct numerical simulations of the Taylor-Couette dynamo. In a first part, we have shown that the classical Taylor-Couette flow produces a spatially subharmonic dynamo, i.e., a magnetic field which have axial wavelengths exceeding by a factor two those of the flow pattern. This subharmonic nature of the dynamo have interesting consequences, such as a minimal aspect ratio  $\Gamma = Hd$  below which no dynamo action can be obtained, or the presence of resonant tongues in the marginal stability curve.

We have also studied, for the first time, the effect of the turbulence on the Taylor-Couette dynamo. As observed for many systems, when  $Re$  is increased, the turbulent fluctuations tend to increase the critical threshold  $Rm_c$  of the dynamo. We have shown that when  $Re$  exceeds a few thousands, the velocity field bifurcates to a strongly fluctuating state able to sustain a turbulent dynamo. However, some coherence of the Taylor vortices is still needed in this turbulent regime, and the dynamo tends to disappear at very large Reynolds number.

Based on the observation that the Taylor-Couette dynamo is a subharmonic dynamo related to Taylor vortices, we have proposed new configurations that may be very efficient in the context of a laboratory dynamo experiment. By attaching some additional rings to the cylinders, it is possible to generate powerful and coherent Taylor-like vortices. This artificial boundary-driven cellular flow generates velocity amplitudes much larger than the Taylor-Couette cells, providing dynamo threshold remarkably small. This is an interesting perspective for a large scale dynamo experiment.

On the other hand, since the calculations reported here clearly show that the turbulence tends to inhibit dynamo action, it is crucial to understand the effect of turbulent fluctuations on these artificial flows. Because of the geometrical constraint, one may expect these flows to be more coherent at large  $Re$  than the classical Taylor vortices. A complete investigation of these artificial flows at large  $Re$  will therefore be addressed in a future work.

Similarly, it would be interesting to study how the rotation of the outer cylinder may help sustaining the coherence of Taylor vortices in the turbulent regime. Since the Taylor-Couette flow provides a very strong analogy with the thermal convection instability, a study of dynamos generated by turbulent Taylor-Couette flows with global rotation could be very helpful to the investigation of planetary dynamos. In addition, one should note that these numerical simulations have been done with a compressible code. Although our calculations were done with low Mach numbers, it would be interesting to understand how our results depend on the compressibility of the flow.

## ACKNOWLEDGMENTS

The author would like to sincerely thank Hantao Ji, Stephan Fauve, and Jeremy Goodman for their very constructive comments and suggestions. Calculations were performed at TGCC center.

- <sup>1</sup> See, for instance, H. K. Moffatt, *Magnetic Field Generation in Electrically Conducting Fluids* (Cambridge University Press, Cambridge, 1978); E. Dormy and A. M. Soward, *Mathematical Aspects of Natural Dynamos* (CRC Press, Boca Raton, 2007).
- <sup>2</sup> G. Rüdiger, L. Kitchatinov, and R. Hollerbach, *Magnetic Processes in Astrophysics* (Wiley-VCH, 2013).
- <sup>3</sup> A. Willis and C. Barenghi, *Astron. Astrophys.* **393**, 339–343 (2002).
- <sup>4</sup> P. Laure, P. Chossat, and F. Daviaud, in *Dynamo and Dynamics: A Mathematical Challenge*, Nato Science Series II Vol. 26 (Springer, Berlin, 2000), pp. 17–24.
- <sup>5</sup> J. L. Guermond, R. Laguerre, J. Leorat, and C. Nore, *J. Comput. Phys.* **228**, 2739–2747 (2009).
- <sup>6</sup> S. Colgate *et al.*, *Phys. Rev. Lett.* **106**, 175003 (2011).
- <sup>7</sup> H. Ji *et al.*, *Nature (London)* **444**, 343 (2006); F. Stefani *et al.*, *Phys. Rev. Lett.* **97**, 184502 (2006).
- <sup>8</sup> M. González *et al.*, *Astron. Astrophys.* **464**, 429–435 (2007).
- <sup>9</sup> W. Liu, J. Goodman, and H. Ji, *Astrophys. J.* **643**, 306 (2006).
- <sup>10</sup> W. Liu, *Astrophys. J.* **684**, 515 (2008).
- <sup>11</sup> C. Gissinger, H. Ji, and J. Goodman, *Phys. Rev. E* **84**, 026308 (2011).
- <sup>12</sup> T. Benjamin, *Proc. R. Soc. London, Ser. A* **359**, 1–26 (1978); *Proc. R. Soc. London, Ser. B* **359**, 27–43 (1978); T. Benjamin and T. Mullin, *Proc. R. Soc. London, Ser. A* **377**, 221–249 (1981).
- <sup>13</sup> S. Balbus and J. Hawley, *Astrophys. J.* **376**, 214–233 (1991); E. P. Velikhov, *J. Sov. Phys. JETP* **36**, 995 (1959); S. Chandrasekhar, *Proc. Natl. Acad. Sci. U.S.A.* **46**, 253 (1960).
- <sup>14</sup> F. Rincon *et al.*, *Phys. Rev. Lett.* **98**, 254502 (2007).
- <sup>15</sup> S. Chandrasekhar, *Hydrodynamic and Hydromagnetic Stability* (Clarendon, Oxford, 1961).

- <sup>16</sup> A. Tilgner and F. Busse, *Proc. R. Soc. London, Ser. A* **448**, 237–244 (1995).
- <sup>17</sup> F. Plunian and K. Rädler, *Geo. Astron. Fluid Dyn.* **96**, 115–133 (2002).
- <sup>18</sup> C. Nore *et al.*, *Phys. Fluids* **24**, 094106 (2012).
- <sup>19</sup> B. Dubrulle *et al.*, *New J. Phys.* **9**, 308 (2007).
- <sup>20</sup> Y. Ponty *et al.*, *New J. Phys.* **9**, 296 (2007).
- <sup>21</sup> A. Schekochihin, *New J. Phys.* **9**, 300 (2007).
- <sup>22</sup> R. Stieglitz and U. Muller, *Phys. Fluids* **13**, 561 (2001).
- <sup>23</sup> A. Gailitis *et al.*, *Phys. Rev. Lett.* **86**, 3024 (2001).
- <sup>24</sup> R. Monchaux *et al.*, *Phys. Rev. Lett.* **98**, 044502 (2007).
- <sup>25</sup> C. Collins, *Phys. Rev. Lett.* **108**, 115001 (2012).